Numerical Model to Estimate the Potential Changes within Laser-Solid Surface Interaction Zone

Noor I. Naji
Abdul-Mutalib I. Ahmed

School of Applied Sciences,
University of Technology,
Baghdad, Iraq

In this work, a model is proposed to provide an estimation of the temporal and spatial changes of the potential within the interaction zone between laser and metal surface. The model depends on the real experimental data which were measured around the interaction zone. This model provides an estimation of the charge involved and considers the presence of the hole created by the interaction. For the first time, it provides the spatial and the temporal variation of the potential which reflects the electric forces and temperature at the interaction zone. It also gives a clear insight of the position of the Knudsen layer. The estimated maximum potential is more than ten times the potential at the surface boundary. This implies that surface potential is due to the interaction of the surface with the plasma rather than the usually believed thermionic emission.

Keywords: Laser-solid interaction, Poisson's equation, Knudsen layer, Plasma dynamics
Received: 16 April 2010, **Revised**: 28 May 2010, **Accepted**: 4 June 2010

1. Introduction

When intense laser radiation impinges on a solid target with initial density ρ_s, hot plasma is formed at the surface. Above certain threshold intensity, depending on the wavelength of the laser and material properties, breakdown occurs, i.e., free electrons are created in the irradiated material [1]. Up to date, the procedure, by which the very first free electron is produced, is not recognized precisely. The photon energy of the laser light is not nearly high enough to ionize the atoms or molecules, so direct photoionization cannot occur. As well, the photon energy of laser light is not high enough for multi-photon ionization. Other ionization mechanisms have been proposed, such as stimulated Raman scattering (SRS) [2]. It is most likely, that due to background radiation or impurity effects, free electrons are already present. Whatever the origin of the initial electron, it collides with another atom and ionizes it, creating yet another free electron. One electron becomes multiple electrons, each gaining energy from the radiation field and then ionizing other atoms. The concentration of free electrons increases rapidly and at high enough light intensities, results is the formation of a strongly absorbing layer at the surface of the target.

In order to produce any effect on the material by the laser radiation, laser light must be absorbed. A laser-induced process is thermally activated if the thermalization of the extinction excitation energy is fast compared to the initial processing step (i.e., pulse duration) [3-8]. In such a case, laser treatment is thermal and the laser is simply considered as a heat source. In metals, light is absorbed within 10^{-10}-10^{-14}s [9].

As the laser energy is absorbed, it is transformed into thermal energy by the plasma electrons which carry the energy deeper into the target by electron heat diffusion. At the same time, expansion of the heated material sets in and leads to the formation of an ablative electron heat wave. In a high-Z material, competition between electron heat conduction and conversion into primary x-rays modifies this heat wave. The conversion layer, typically has a high temperature (~1keV) and a low density (~0.1g/cm^3) and is thereby optically thin to the radiation generated there [10].

Focusing a strong laser beam into plasma can considerably influence the plasma's electron temperature and density. This renders the measured values of these parameters useless. The electric field of the intense laser beam can heat electrons in the plasma. This takes place via the process of inverse Bremsstrahlung, which will be introduced later. Kunze [11] estimated the relative change in electron temperature due to heating by the laser beam. The laser pulse length

 ISSN 1813-2065 Printed in IRAQ

is assumed to be long enough to heat the electrons, but too short for the electrons to transfer this heat to the heavy particles. This estimation assumes the laser beam not to affect the absorption coefficient of plasma. This is true if the maximum kinetic energy that a free electron can gain in the radiation field is less than the photon energy [12].

2. Modeling

The Poisson's equation for potential inside the plasma can be written as:

$$\nabla^2 V = -\frac{\rho}{\varepsilon_\circ} \qquad (1)$$

where ∇^2 is the Laplacian operator, V is the potential and ρ is space charge density.

There are many elegant analytical solutions to Poisson's equation in special geometries, but nowadays, real problems are usually solved numerically. Computers and software are now so powerful that it can be easier to obtain a computer solution than to find the exact one in reference books. The finite-difference method (FDM) was used to give the governing partial differential equation for a particular electromagnetic problem. The first step involved in the application of the FDM is [13] dividing the domain of interest into a grid (usually rectangular) in one, two or three dimensions; $V(x,y,z)$, which is a three dimensional (3D) solution, $V(x,y)$, which is a two dimensional (2D) solution (no z-variation), and $V(x)$, which is a one dimensional (1D) solution (no y or z-variation). The second step is developing algebraic equations, which approximate the partial derivatives in the governing equations (difference equations). The final step is solving the set of algebraic equations.

To solve the Poisson's equation numerically, the region of interest can be divided into rectangular grid over which the difference equation approximations to the 2nd order derivatives are defined. The grid points located on the boundaries represent fixed nodes where the potential is known [13,14]. The internal grid points from the boundary are defined as free nodes where the potential must be computed. The grid points are labeled in the x-direction as i, i+1, i+2, etc, and in the y-direction j, j+1, j+2, etc. In other words, we will write the equations at all internal nodes of a grid with a regular step size, h, in the x-direction as Δx, and in the y-direction, as Δy as shown in Fig. (1).

In order to solve Poisson's equation, finite differences method (FDM) is used, and the approximations to model the governing equation are based on forward-difference in time and central-difference in space. The 2D Poisson's equation in rectangular coordinates is [15]:

$$\nabla^2 V = \frac{\partial^2 V}{\partial x^2} + \frac{\partial^2 V}{\partial y^2} = -\frac{\rho}{\varepsilon_\circ} \qquad (2)$$

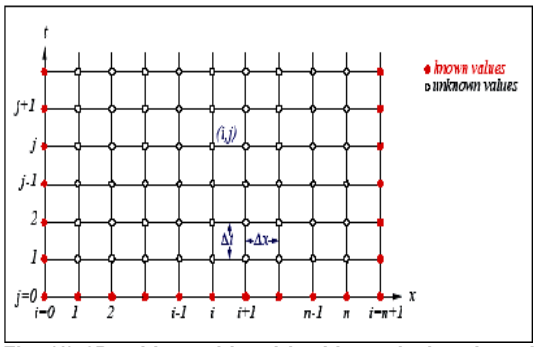

Fig. (1) 2D grid considered in this analysis, where *i* is spatial index and *j* temporal index [13]

Considering a rectangular region defined by $0 \le x \le a$ and $0 \le y \le b$ enclosed by conductors of known potential $V(x,y)$ and known charge distribution throughout $\rho(x,y)$, the required derivatives in the 2D Poisson's equation are:

$$\frac{\partial^2 V}{\partial x^2} = \frac{\partial}{\partial x}\left(\frac{\partial V}{\partial x}\right) \text{ and } \frac{\partial^2 V}{\partial y^2} = \frac{\partial}{\partial y}\left(\frac{\partial V}{\partial y}\right) \qquad (3)$$

The 1st order partial derivatives with respect to x and y can first be defined on either side of the grid point (i,j) as:

$$\left.\frac{\partial V}{\partial x}\right|_{i-\frac{1}{2},j} \approx \frac{V_{i,j} - V_{i-1,j}}{\Delta x} \qquad \left.\frac{\partial V}{\partial y}\right|_{i,j-\frac{1}{2}} \approx \frac{V_{i,j} - V_{i,j-1}}{\Delta y}$$

$$\left.\frac{\partial V}{\partial x}\right|_{i+\frac{1}{2},j} \approx \frac{V_{i+1,j} - V_{i,j}}{\Delta x} \qquad \left.\frac{\partial V}{\partial y}\right|_{i,j+\frac{1}{2}} \approx \frac{V_{i,j+1} - V_{i,j}}{\Delta y}$$

The approximations of the 1st order derivatives on either side of grid point (i,j) can then be used to approximate the 2nd order partial derivatives with respect to x and y as:

$$\left.\frac{\partial^2 V}{\partial x^2}\right|_{i,j} \approx \frac{\left.\frac{\partial V}{\partial x}\right|_{i+\frac{1}{2},j} - \left.\frac{\partial V}{\partial x}\right|_{i-\frac{1}{2},j}}{\Delta x} \qquad (4a)$$

$$\left.\frac{\partial^2 V}{\partial y^2}\right|_{i,j} \approx \frac{\left.\frac{\partial V}{\partial y}\right|_{i,j+\frac{1}{2}} - \left.\frac{\partial V}{\partial y}\right|_{i,j-\frac{1}{2}}}{\Delta y} \qquad (4b)$$

Inserting the 1st order derivative approximations and collecting terms yields the 2nd order derivative approximations, yield

$$\left.\frac{\partial^2 V}{\partial x^2}\right|_{i,j} \approx \frac{1}{\Delta x^2}[V_{i+1,j} - 2V_{i,j} + V_{i-1,j}] \qquad (5a)$$

$$\left.\frac{\partial^2 V}{\partial y^2}\right|_{i,j} \approx \frac{1}{\Delta y^2}[V_{i+1,j} - 2V_{i,j} + V_{i-1,j}] \qquad (5b)$$

Inserting the 2nd order derivative approximations in Poisson's equation gives:

$$\frac{V_{i+1,j} - 2V_{i,j} + V_{i-1,j}}{\Delta x^2} + \frac{V_{i,j+1} - 2V_{i,j} + V_{i,j-1}}{\Delta y^2} = -\frac{\rho}{\varepsilon_\circ} = B \qquad (6)$$

Given a square grid ($\Delta x = \Delta y = h$), the equation above is reduced to:

$$V_{i+1,j} + V_{i-1,j} + V_{i,j-1} - 4V_{i,j} = -\frac{h^2 \rho_{i,j}}{\varepsilon_\circ} \qquad (7)$$

which is a square-grid 2D Poisson's equation

3. Experimental and Model Assumptions

Previous experimental results [16-21] were used for feeding the mathematical model with the required data to solve the equations involved. A solid stainless-steel 304 sample was irradiated by Nd:YAG laser pulses with intensity of I=12.4MW/cm^2 and wavelength λ=1.069μm. The laser was focused on spot of area A=1.38x10^{-3}cm^2 using a 10cm focusing lens [17]. A surface voltage is generated during the interaction between laser pulse and the sample [20]. A floating potential probe was used at a distance 3mm away from the sample surface to measure the potential of the plasma generated [18].

To start the analytical modeling of the experimental results, as well as to provide a solution of the problem, several assumptions are made. The material is considered as a layer that first melts then evaporates, where the skin depth represents thickness of this layer and the spot area represents the area of this layer. The system is placed into an evacuated chamber where the right and left boundary voltages (V_{bR} and V_{bL}) are zero by neglecting the charge loss produced from attraction of charge with surface. Therefore, the net charge, not the positive or the negative charge, is considered because the data taken from reference [52] represent the net charge. As well, the ionization by absorption is neglected. Also, no time delay between the charge at the boundary and the interaction zone occurs. This is needed for proper time analysis. As well, the charge is not accumulated at the interaction zone. This is true only for high vacuum. We assume that the problem is spatially 3D (x,y,z) and because of symmetry around z we have considered (x,z) for simplicity and reducing matrix size and time of calculation. We have used Cartesian coordinates because the charge distribution and motion is not a point source or cylindrical.

4. Model Parameters

The considered model needs many predefined parameters as well as numerical solutions of Poisson's equation.

4.1 Boundary Conditions Consideration

The values of the boundary conditions are taken as:

(a) Metal surface potential boundary data values are provided by reference [20]. This potential is generated from the reaction of the St-St. 304 sample with the Nd:YAG laser pulses of incident intensity 12.4 MW/cm^2. Using least square fitting (LSF) to represent these results with polynomials yields:

$V_1(t)$ = 8.758231326297914e+023t^6 - 9.647570877481166e+020t^5 + 4.3214683770712e+017t^4 + 1.004569463264522e+014t^3 + 1.274971036417507e+010t^2 - 8.371153279949487e+005t + 2.221652415436611e+001 *for* $0 \le t \le t_1$

$V_2(t)$ = -4.216190398182638e+010t^3 + 4.106638304623091e+007t^2 - 1.283412744333760e+004t + 1.211358590639905e+000 *for* $t_1 \le t \le t_2$

$V_3(t)$ = 1.058336673315529e+00t^2 - 8.700171524786168e+001t - 3.133347479914106e-002 *for* $t_2 \le t \le t_3$

where t_1, t_2 and t_3 are selected times on the potential-time curve

---

(b) The boundary data at a distance of 3mm away from the surface is taken from the experimental result of reference [18], which measured the temporal voltage using three floating probes: one single cylindrical and two circular (4.5mm and 9mm in diameter). These results are collected and interpolated as temporal and spatial voltages and they represent the potential over a lateral distance of 9mm.

The dimensions of the target are 5×2mm^2, therefore, we have selected the potentials over a central distance of 5mm instead of 9mm and for the same durations. They are considered as the upper boundary conditions.

4.2 The Charge Consideration

We get the values of the charge density from two resources; the first is the values of charge density for different time and space from the center point where the laser interaction with solid. We have integrated the data as:

$$\rho(t) = \int_{x=-4.9}^{4.9} \rho(x,t)dx \qquad (8)$$

This charge is assumed to exist in the hole based on the following assumption from charge reservation law:

$$Q_{probe} = Q_{hole}$$
$$\rho_{probe} A_{probe} = \rho_{hole} A_{hole} \qquad (9)$$

ISSN 1813-2065 Printed in IRAQ

where ρ_{probe}, ρ_{hole} and A_{probe}, A_{hole} are charge densities and surface areas of probe and hole, respectively

This charge may be distributed on the first layer of the hole, or overall the layers of the hole.

For the first layer

$$\left(\frac{\int \rho_{probe}}{H_{w1st}}\right)(L_{probe}t_{probe}) = \rho_{hole}(hkH_w) \quad (10a)$$

where H_{w1st} and H_w are the number of points of 1st layer (hole) and one layer, respectively, L and t are the length and thickness of the probe, respectively

For all layers

$$\left(\frac{\int \rho_{probe}}{H_{wall}}\right)(L_{probe}t_{probe}) = \rho_{hole}(hkH_w) \quad (10b)$$

The second resource is using thermal emission as we have calculated the total current density as:

$$J = A^* T^2 exp\ (-E_\omega / k_b T) \quad (11)$$

where A^* is Richardson constant, T is the temperature, E_ω is the work function. The electronic current density can be obtained by:

$$J_e = A^* T^2\ exp\ (-E_\omega / k_b T) = 138.936\ \text{A/cm}^2$$
$$I = J \text{ x } A = 736.365036397\text{x}10^{-3}\ \text{A}$$
$$Q = I \text{ x } t_{layer} = 3788.64252135\text{x}10^{-9}\ \text{C}$$

The charge appears to be very small compared to that calculated from probe measurements. Therefore, we use the charge from these probe measurements.

4.3 Hole Size Consideration

Both fixed hole size of (1x1) mm and variable hole size can be considered. It was taken from previous heat model of reference [21] who considered removing a skin layer according to the deposited variable heat delivered by the laser source. The number of layers is temporally varied and changes as:

$$\frac{\Delta n}{\Delta t} = -9.6938e+024t^6 + 2.6055e+023t^5 - 6.3024e+020t^4 + 6.1694e+017t^3 - 2.9029e+014t^2 + 5.6906e+010t + 30932$$

We have derived the size from the following equation:

Z_H (size of hole) = n_L (number of layers at that time) x Z_L (size of layer)

where Z_L (size of layer) = δ (skin depth) x A (spot area)

The skin depth = 10^{-7}cm, and the spot area = $1.38\text{x}10^{-3}\text{cm}^2$.

This is satisfactory if we are looking for the variation of voltage over all space over the surface up to upper boundary.

5. Results and Discussion

The potential over the surface up to the boundary is derived by solving Poisson's equation numerically

$$\nabla^2 V = -\frac{\rho}{\varepsilon_\circ} \quad (12)$$

The 2D Poisson's equation in rectangular coordinates is

$$\nabla^2 V = \frac{\partial^2 V}{\partial x^2} + \frac{\partial^2 V}{\partial y^2} = -\frac{\rho}{\varepsilon_\circ} \quad (13)$$

according to the numerical analysis given in advance. A nodal grid is created and used in the derivation of the finite difference equations. A grid is spaced every $5\text{x}10^{-3}$/d cm along the horizontal and vertical axis to ensure that at least 31 nodes are used in obtaining the potential distribution as shown in Fig. (2).

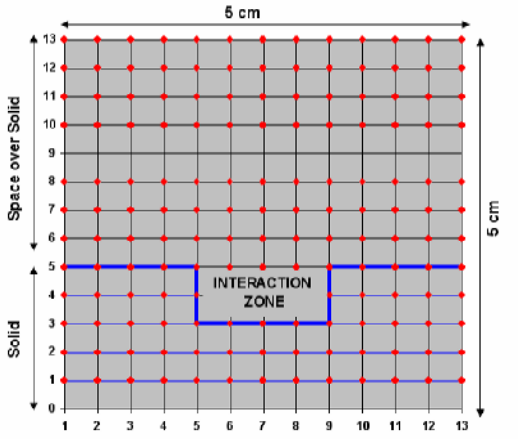

Fig. (2) Nodal grid formed in order to derive the finite difference equations

We have used 31×31 grid size to represent reasonably the actual size 5×5mm and 2mm of the metal surface. Execution of a program with this size of grid is fast since matrix size is not large. Although the program is made flexible to any size, but MATLAB for larger size would be slow.

The charges collected on the probes are considered to be the same as in the hole. This is calculated as:

$$Q_{(t)} = \rho_{probe\,(t)} L = \rho_{hole\,(t)} W \quad (14)$$

where L is the boundary length, W is the hole length, $\rho_{probe(t)}$ is the temporal charge density on the probe and $\rho_{hole(t)}$ is the temporal charge density in the hole

This charge may be divided equally on the first layer of the hole points or may be divided entirely over all the hole size (2D).

Analysis of the plasma potential production from interaction of a laser beam with a workpiece is based on development of a two-dimensional model for the geometry shown in Fig. (3). The laser beam is characterized by its wavelength λ, the beam spot radius ω_0 at the

surface, the skin depth δ, and the power density I within the spot. The workpieces were secured by a rectangular plate with a square hole in the middle, so that the laser beam could irradiate the exposed workpiece in the middle of the clamp plate.

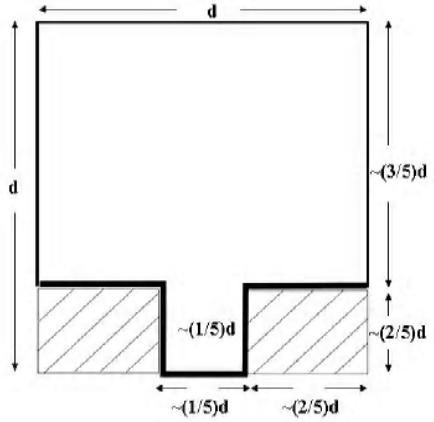

Fig. (3) Description of the boundary conditions of the mathematical model used in this work

The model described in this work explains a physical matter that can be described as a material (St. St. 304) of 2mm thickness and 5mm length, three probes (single cylindrical, and two ring probes of 9mm and 4.5mm diameters) at a distance of 3mm from the target, where the values produced from these probes were assumed as boundary conditions for the upper limits of the model and the boundary condition of the lower limit of the model was taken from reference [17]. Finally, the boundary conditions on the left and right side of the mathematical model has been assumed zero considering that the system is located in an evacuated chamber. The results have taken into account all the variables mentioned above according to the block diagram shown in Fig. (4).

The problem is solved with charge density Poisson's equation. We have solved the problem when the charge density is in the first layer and we consider a fixed hole size (1×1mm) and with only metal surface potential boundary data values as shown in Fig. (5).We have also solved the problem in the same case as before but with metal surface potential boundary data values and with boundary data at 3mm away from the surface as shown in Fig. (6).

The problem is solved when the charge density is in all layer and we consider a fixed hole size (1×1mm) and with only metal surface potential boundary data values as shown in Fig. (7).We have also solved the problem in the same case as before but with metal surface potential boundary data values and with boundary data at 3mm away from the surface as shown in Fig. (8).

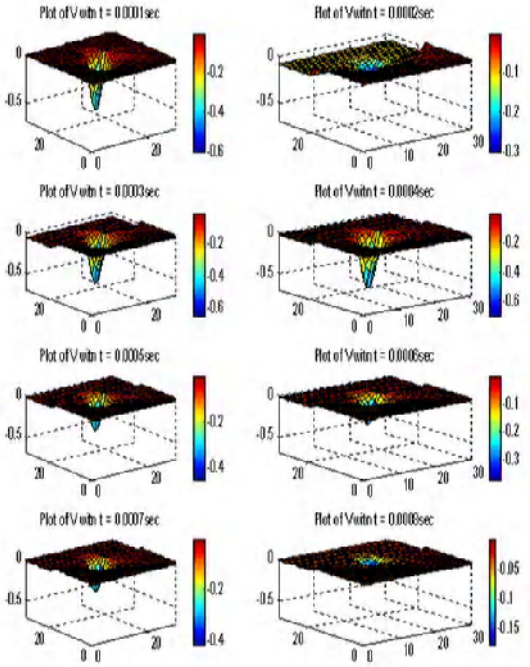

Fig. (5) The solution of the problem when the charge density is in the first Layer and considering a fixed hole size (1×1mm) and with only metal surface potential boundary data values

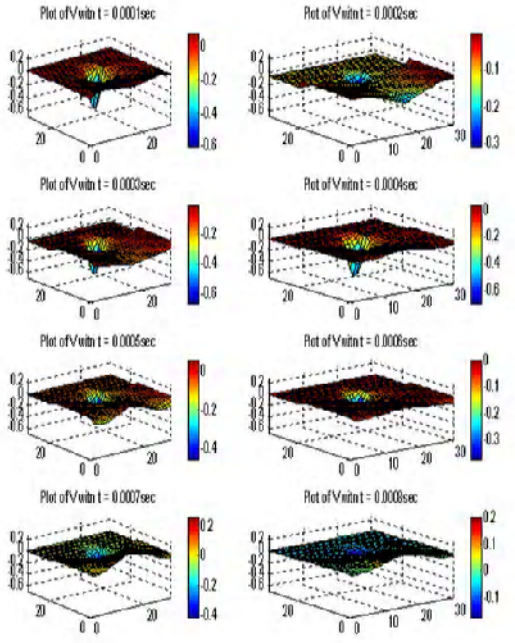

Fig. (6) The solution of the problem in the same case as before but with metal surface potential boundary data values and with boundary data a 3mm away from the surface

We also have solved the problem with hole, and we may consider a variable hole size with time but with only metal surface potential boundary data values as shown in Fig. (9). We have solved the problem in the same case as before but with metal surface potential boundary data values and with boundary data at 3mm away from the surface as shown in Fig. (10).

The case in Fig. (5) represents the potential in vacuum with no upper boundary condition. Also it represents a true experimental case at the early stage of the pulse where the mass removal is small (no proper hole).The variation of the potential with time shows clearly the stages of plum dynamic. The maximum voltage peak is about ten times the voltage of the surface boundary at t=0.001sec. At all other times the surface potential does not affect the plasma potential but only in the part near the surface.

The upper boundary in Fig. (6) does not influence the result of Fig. (5). This reflects that the potential peak near the surface is not smoothed by the upper boundary. The effect of the boundary is to change the potential distribution near the boundary since the charge is distributed in the boundary over a very large distance compared to the interaction zone.

The hole creation usually represents the extraction process that starts rapidly at the beginning of the pulse, then decays with pulse decay. Although we have assumed a constant size (1×1mm) which represents the ultimate size. The presence of hole seems to influence the potential distribution since the changes will be distributed over a greater area. The maximum peak is about 30 times the peak of the surface boundary. The effect of upper boundary in Fig. (8) only influences the region close to the boundary. This is same as in Fig. (6).

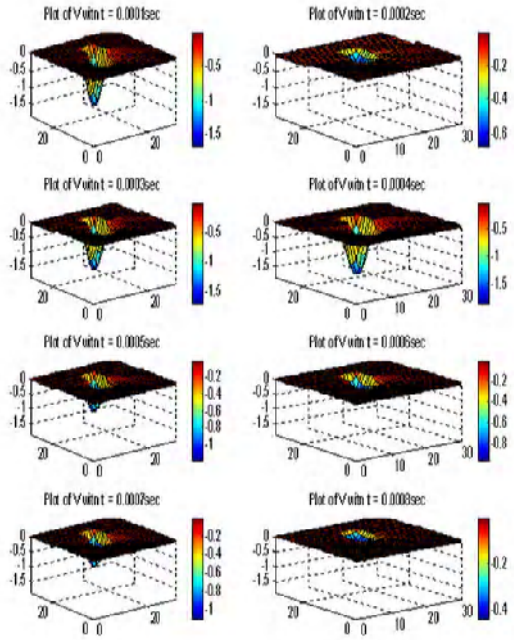

Fig. (7) The solution of the problem when the charge density is in all Layers and considering a fixed hole size (1×1mm) and with only metal surface potential boundary data values

The case of Fig. (9) represents the actual simulation of the interaction process, where the created hole size depends on the laser intensity. The potential appears to stay almost constant but the width varies with size of the hole. The width of the potential always increases with hole size.

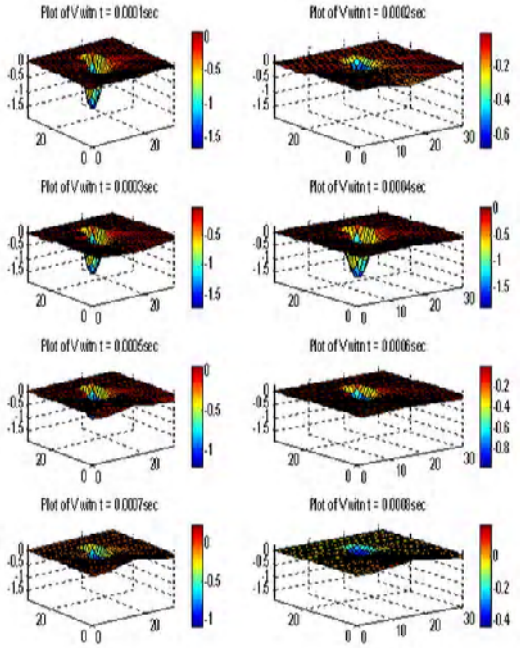

Fig. (8) The solution of the problem in the same case as before but with Metal surface potential boundary data values and with boundary data at 3mm away from the surface

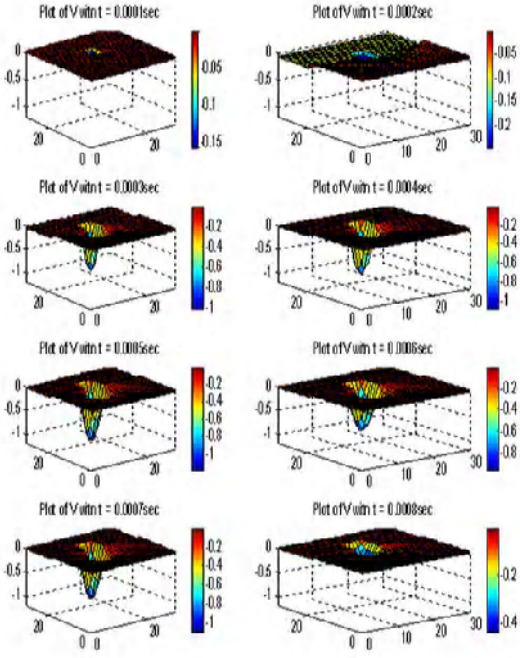

Fig. (9) The solution of the problem with hole, and we may consider a variable hole size with time but with only metal surface potential boundary data values

The effect of applying upper boundary with dynamic hole creation is presented in Fig. (10).

This boundary still only influence the region close the boundary, as in Fig. (6) and Fig. (8).

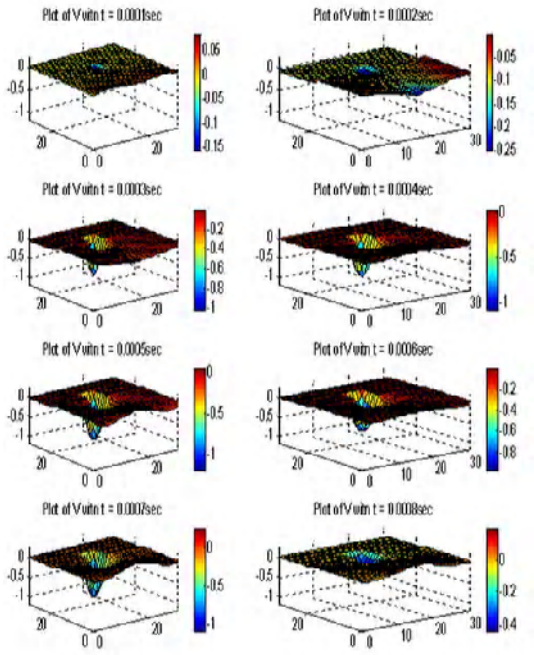

Fig. (10) The solution of the problem in the same case as before but with metal surface potential boundary data values and with boundary data at 3mm away from the surface

6. Conclusions

According to the results obtained from this work, we can conclude that a large change in the potential values appears within the interaction zone. This will cause a large electric field. This means that there is a large force acts on the charges leading to a large acceleration and collision and therefore provides good ionization and absorption conditions. As well, the most important advantage of this method is to clearly define the position of the Knudsen layer, which defines the region where the density, velocity and pressure change dramatically. We believe that this layer could be studied further using this potential method. For comparison, we have calculated the potential where boundary voltage, charge and hole are removed. The estimated maximum potential peak is ten times the surface potential. This definitely concludes that the surface potential is not a thermoionic emission type. This is also supported by the small calculated charge derived from thermoionic emission in this work. If we consider that the charge exists not only on the first layer but in all layers, then there is a large change in potential arise, whose width is proportional to hole size. The amount of the potential gradient depends on the charge. The symmetry of the potential distribution is affected by the boundary condition, while the value of the potential is proportional to it.

References

[1] Hoar, H., **"Physics of Laser Driven Plasmas"**, John Wiley & Sons (NY), 1981.

[2] Salcedo, A. et al., *"Studies of stimulated Raman scattering in laser plasma interactions"*, *Private communications*, 2002.

[3] Borghesi, M. et al., *Phys. Rev. E*, 54(6) (1996) 6769-6773.

[4] Gizzi, L.A. et al., *Laser and Particle Beams*, 19 (2001) 181-186.

[5] Galemberti, M. et al., *Laser and Particle Beams*, 19 (2001) 47-53.

[6] Borghesi, M. et al., *Phys. Rev. Lett.*, 88(13) (2002) 1- 4.

[7] Borghesi, M. et al., *Phys. of Plasma*, 9(5) (2002) 2214-2220.

[8] Tomassini, P. et al., *Phys. of Plasma*, 10(4) (2003) 917-920.

[9] Miyamoto, K., **"Fundamentals of Plasma Physics and Controlled Fusion"**, University of Tokyo (Japan), 2000.

[10] Rytter, M., *"A study of the production and characterization of a laser generated soft x-ray source"*, M.Sc. thesis, University of Southern Denmark (Denmark, 2003).

[11] Van de Sande, M.J., *"Laser scattering on low temperature plasmas High resolution and stray light rejection"*, Ph.D. thesis, Technical University of Eindhoven (Netherlands, 2002).

[12] Jonkers, J., Bakker, M. and van der Mullen, J.A.M., *J. Phys. D: Appl. Phys.*, 30 (1997) 1928.

[13] "*Numerical Solution of the Transient Diffusion Equation using the Finite Difference Method*", report at www.research.ibm.com/jourrnal/rd/444/jordansweet.html

[14] Eliasson, B., *"Numerical of Vlasov-Maxwell Modeling of Space Plasma"*, Ph.D. Thesis, 2002, Uppsala University, Sweden.

[15] "*Finite Difference Technique*", report at www.research.ibm.com/jourrnal/rd/444/jordansweet.html

[16] Abed, A.-H.M., *"Effect of plasma on the efficiency of laser machining (drilling)"*, M.Sc. thesis, University of Technology, Baghdad (1984).

[17] Ali, S.M., *"Laser-Plasma Interaction"*, M.Sc. thesis, University of Technology, Baghdad (1992).

[18] Essam, M.B., *"The electrical nature of the medium generated from laser-material interaction"*, M.Sc. thesis, University of Technology, Baghdad (1994).

[19] Mubarak, T.H., *"The transmission of laser through the interaction region with materials at different pressures and gases"*,

 ISSN 1813-2065 Printed in IRAQ

M.Sc. thesis, University of Technology, Baghdad (1984).
[20] Al-Qaisy, S.Q., *"Studying the surface charge resulted from plasma generated from its interaction with laser"*, M.Sc. thesis, University of Technology, Baghdad (1995).
[21] Aseel, M., *"Study into thermal effect of laser interaction with solid surface"*, M.Sc. thesis, University of Technology, Baghdad (2005).

Reviewing codes: AP0214/2010/01/IND, AP0214/2010/02/CHN

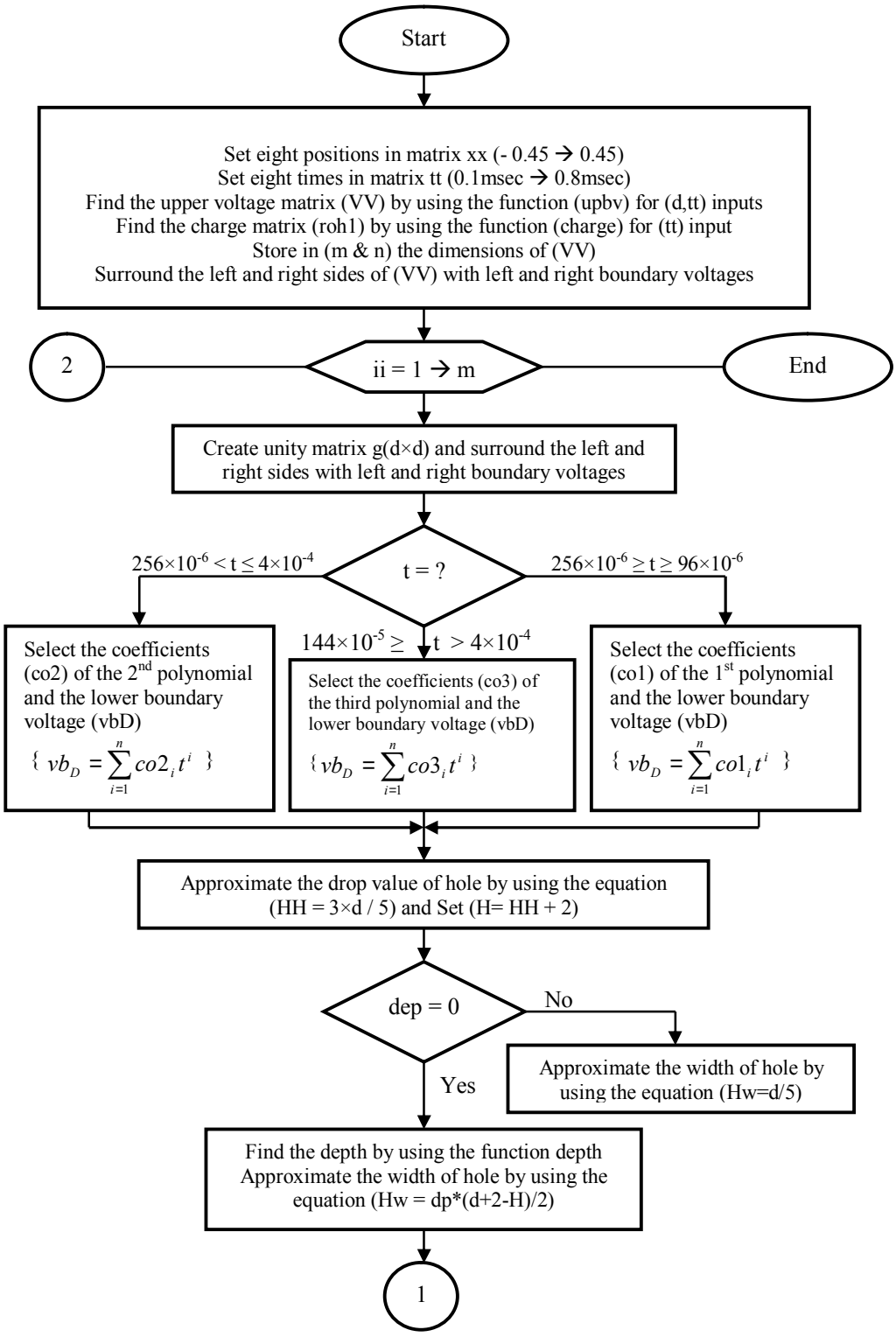

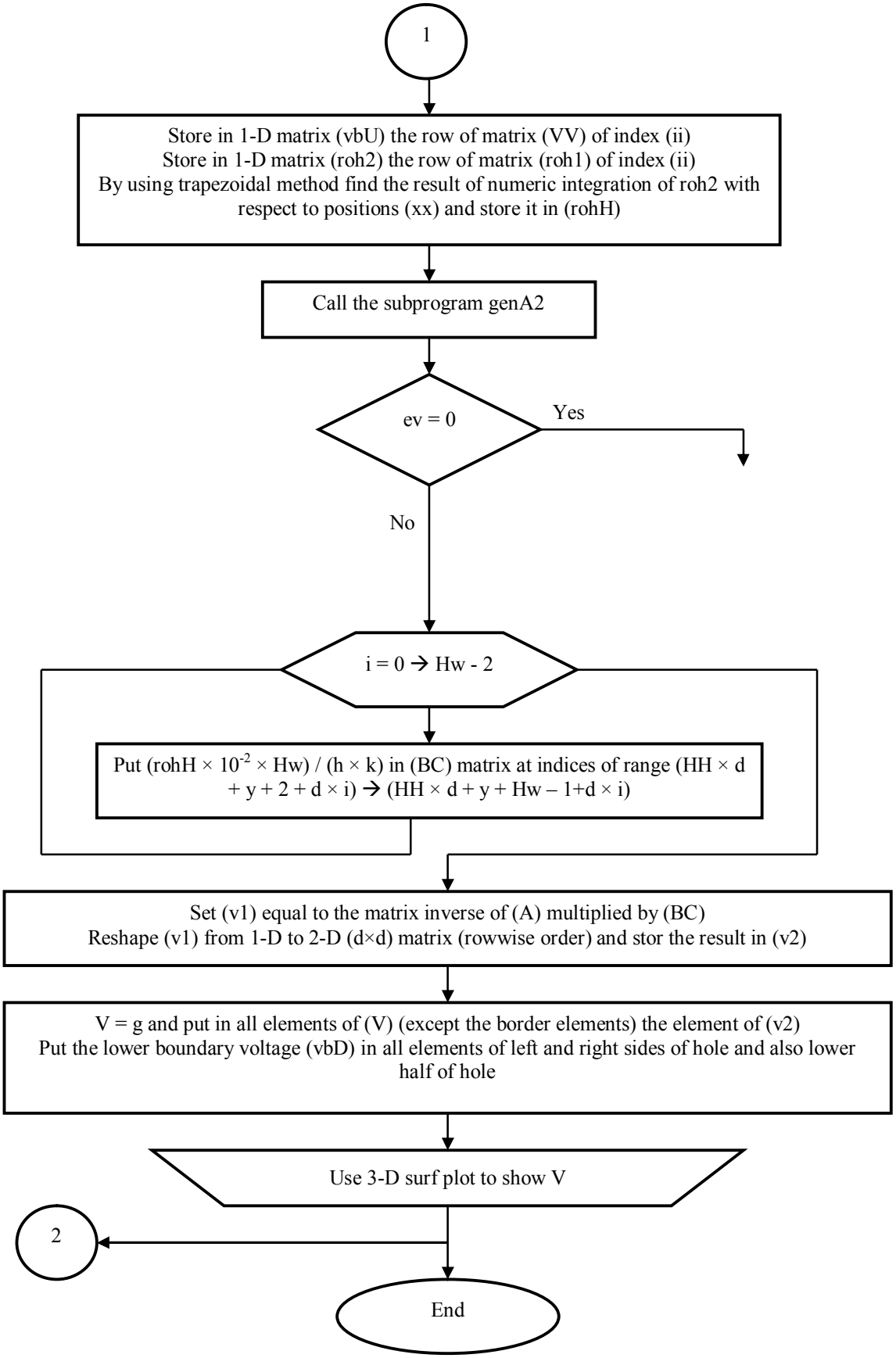

Fig. (4) Flow chart for the numerical solution of Poisson's equation

ISSN 1813-2065 Printed in IRAQ